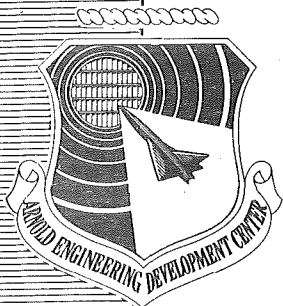


AEDC-TR-85-63



# Estimating Water Vapor Condensation Effects for Transonic and Supersonic Flow Fields

C. E. Robinson and R. C. Bauer  
Calspan Corporation

December 1985

Final Report for Period 1 October 1982 – 31 August 1985

Approved for public release; distribution unlimited.

**ARNOLD ENGINEERING DEVELOPMENT CENTER  
ARNOLD AIR FORCE STATION, TENNESSEE  
AIR FORCE SYSTEMS COMMAND  
UNITED STATES AIR FORCE**

## NOTICES

When U. S. Government drawings, specifications, or other data are used for any purpose other than a definitely related Government procurement operation, the Government thereby incurs no responsibility nor any obligation whatsoever, and the fact that the government may have formulated, furnished, or in any way supplied the said drawings, specifications, or other data, is not to be regarded by implication or otherwise, or in any manner licensing the holder or any other person or corporation, or conveying any rights or permission to manufacture, use, or sell any patented invention that may in any way be related thereto.

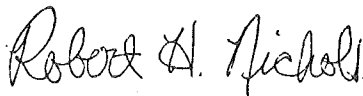
Qualified users may obtain copies of this report from the Defense Technical Information Center.

References to named commercial products in this report are not to be considered in any sense as an endorsement of the product by the United States Air Force or the Government.

This report has been reviewed by the Office of Public Affairs (PA) and is releasable to the National Technical Information Service (NTIS). At NTIS, it will be available to the general public, including foreign nations.

## APPROVAL STATEMENT

This report has been reviewed and approved.



ROBERT H. NICHOLS  
Directorate of Technology  
Deputy for Operations

Approved for publication:

FOR THE COMMANDER



LOWELL C. KEEL, Lt Colonel, USAF  
Director of Technology  
Deputy for Operations

UNCLASSIFIED

SECURITY CLASSIFICATION OF THIS PAGE

REPORT DOCUMENTATION PAGE				
1a. REPORT SECURITY CLASSIFICATION UNCLASSIFIED		1b. RESTRICTIVE MARKINGS		
2a. SECURITY CLASSIFICATION AUTHORITY		3. DISTRIBUTION/AVAILABILITY OF REPORT		
2b. DECLASSIFICATION/DOWNGRADING SCHEDULE		SEE REVERSE OF THIS PAGE		
4. PERFORMING ORGANIZATION REPORT NUMBER(S) AEDC-TR-85-63		5. MONITORING ORGANIZATION REPORT NUMBER(S)		
6a. NAME OF PERFORMING ORGANIZATION Arnold Engineering Development Center	6b. OFFICE SYMBOL (If applicable) DOT	7a. NAME OF MONITORING ORGANIZATION		
6c. ADDRESS (City, State and ZIP Code) Air Force Systems Command Arnold Air Force Station, TN 37389-5000		7b. ADDRESS (City, State and ZIP Code)		
8a. NAME OF FUNDING/SPONSORING ORGANIZATION Arnold Engineering Development Center	8b. OFFICE SYMBOL (If applicable) DO	9. PROCUREMENT INSTRUMENT IDENTIFICATION NUMBER		
8c. ADDRESS (City, State and ZIP Code) Air Force Systems Command Arnold Air Force Station, TN 37389-5000		10. SOURCE OF FUNDING NOS.	PROGRAM ELEMENT NO. 65807F	PROJECT NO.
11. TITLE (Include Security Classification) SEE REVERSE OF THIS PAGE		TASK NO.	WORK UNIT NO.	65087E
12. PERSONAL AUTHOR(S) Robinson, C. E., and Bauer, R. C., Calspan Corporation/AEDC Division				
13a. TYPE OF REPORT Final	13b. TIME COVERED FROM 10/1/82 TO 8/31/85	14. DATE OF REPORT (Yr., Mo., Day) December 1985	15. PAGE COUNT 38	
16. SUPPLEMENTARY NOTATION Available in Defense Technical Information Center (DTIC).				
17. COSATI CODES		18. SUBJECT TERMS (Continue on reverse if necessary and identify by block number)		
FIELD	GROUP	SUB. GR.	water vapor	
20	04		transonic airfoils	
20	13		supersonic nozzles	
			condensation reactions	
			enthalpy	
19. ABSTRACT (Continue on reverse if necessary and identify by block number) A computer code has been developed which estimates the effect of water vapor condensation in two- and three-dimensional flow fields using the Euler equations. The program computes the effect by including the energy release due to condensation in the energy equation. In this manner, the local effect of condensation is included in the calculation of the flow-field properties. A species equation for the conservation of water vapor is also included, as well as an empirical method of predicting the onset of condensation. To evaluate the versatility of the code, calculations of the transonic flow field about a two-dimensional airfoil, a cone at angle of attack, and the flow in planar, two-dimensional and axisymmetric supersonic nozzles have been made for discrete values of specific humidity. In general, the effects of local condensation and revaporization estimated by the code are in good agreement with the experimental data found in the literature.				
20. DISTRIBUTION/AVAILABILITY OF ABSTRACT UNCLASSIFIED/UNLIMITED <input type="checkbox"/> SAME AS RPT. <input checked="" type="checkbox"/> DTIC USERS <input type="checkbox"/>		21. ABSTRACT SECURITY CLASSIFICATION UNCLASSIFIED		
22a. NAME OF RESPONSIBLE INDIVIDUAL W. O. Cole		22b. TELEPHONE NUMBER (Include Area Code) (615) 454-7813	22c. OFFICE SYMBOL DOS	

UNCLASSIFIED

SECURITY CLASSIFICATION OF THIS PAGE

3. DISTRIBUTION/AVAILABILITY OF REPORT

Approved for public release; distribution unlimited.

11. TITLE

Estimating Water Vapor Condensation Effects for Transonic and Supersonic Flow Fields

UNCLASSIFIED

SECURITY CLASSIFICATION OF THIS PAGE

## PREFACE

The work reported herein was conducted by the Arnold Engineering Development Center (AEDC), Air Force Systems Command (AFSC). The Air Force project manager was R. H. Nichols. The results of the research were obtained by Calspan Corporation/AEDC Division, operating contractor for the aerospace flight dynamics facilities at the AEDC, AFSC, Arnold Air Force Station, Tennessee. The research was conducted during the period from October 1, 1982 through August 31, 1985 under AEDC Project Number D631PW (Calpsan Project Number P32C-BE). The manuscript was submitted for publication on September 25, 1985.



## CONTENTS

	<u>Page</u>
1.0 INTRODUCTION .....	5
2.0 DESCRIPTION OF HUMID/EULER	
2.1 Basic Equations .....	5
2.2 Source Terms .....	7
2.3 Condensation .....	8
2.4 Initial and Boundary Conditions .....	10
3.0 COMPUTATIONAL GRID GENERATION .....	11
4.0 DISCUSSION OF RESULTS	
4.1 Two-Dimensional Predictions .....	14
4.2 Three-Dimensional Predictions .....	25
5.0 CONCLUSIONS .....	30
REFERENCES .....	31

## ILLUSTRATIONS

### Figure

1. Supercooling as a Function of Nozzle Temperature Gradient .....	9
2. Computational Mesh for NACA-0012 Airfoil .....	11
3. Computational Mesh for Circular Arc Nozzle .....	12
4. Computational Mesh for Three-Dimensional Wing-Body .....	13
5. Computational Mesh for 15-deg Sharp-Nosed Cone .....	14
6. Two-Dimensional Nozzles .....	15
7. Comparison of Predicted Condensation Effects with Experimental Results for a Mach 2.1 Circular Arc Nozzle .....	16
8. Computed Nozzle Exit Mach Number Distribution for Specific Humidities of 0.0 and 0.0049 .....	16
9. Computed Nozzle Total-Enthalpy Distribution at Specific Humidities of 0.0 and 0.0049 .....	17
10. Effect of Humidity on 16S Nozzle Total Pressure .....	18
11. Computed Nozzle Total-Enthalpy Distribution at a Specific Humidity of 0.002 for the 16S Mach 2.5 Contour .....	19
12. Humidity Effects on an NACA-0012 Airfoil .....	19
13. Effect of Local Condensation on Mach Number Contours .....	21

<u>Figure</u>	<u>Page</u>
14. Condensation Onset Location and Percent Mach Number Decrease After Shock as a Function of Specific Humidity .....	22
15. Computed <del>Nozzle</del> Total-Enthalpy Distribution at a Specific Humidity of 0.0025 for the NACA-0012 Airfoil .....	22
16. Profile of Cast-10 Transonic Airfoil .....	23
17. Effect of Model Scale on Normal-Force Coefficient at Constant Specific Humidity .....	23
18. Geometry of APTU Mach 3.5 Nozzle .....	24
19. Computed Nozzle Total-Enthalpy Distribution at a Specific Humidity of 0.012 for the APTU Mach 3.5 Contour .....	24
20. Computed Nozzle Exit Mach Number Distribution for Specific Humidities of 0.0 and 0.0120, Mach 3.5 APTU Nozzle .....	25
21. Comparison of Mach Number of 15-deg Cone Surface with and without Revaporization .....	27
22. Mach Number and Pressure Coefficient Distribution on Lee Side of 15-deg Cone at a Free-Stream Mach Number of 1.15 with and without Revaporization .....	28
23. Comparison of Mach Number on 7.5-deg Cone Surface with and without Revaporization .....	29
24. Humidity Effects on an F-16 Wing-Body as Function of Dew Point Temperature .....	29
 NOMENCLATURE .....	 33

## 1.0 INTRODUCTION

Experimental data obtained in the AEDC Tunnel 16T, with variations of specific humidity in the free-stream flow, have shown a significant effect of humidity on the measured aerodynamic parameters. The effect is most prominent at supersonic Mach numbers; however, a measurable effect has been observed at high subsonic Mach numbers when large regions of supercritical flow exist over the model. The observed effect has caused concern about the effectiveness of the drying criteria now used to define usable test conditions in the wind tunnel. In an attempt to gain an understanding of the effect of humidity, an analytical method of predicting the influences of humidity on an aerodynamic flow field was developed.

The humidity effect is caused by the local condensation of moisture as the flow moves over the wind tunnel model. The local condensation will release heat, thereby affecting the pressure and temperature conditions in the flow field. However, experiments with small nozzles show that a significant amount of supercooling can exist before condensation occurs. The experiments of Lukasiewicz and Royle (Ref. 1) show that the amount of supersaturation is proportional to the temperature gradient in the flow and hence is a function of the size of the wind tunnel model. Therefore, one would expect less supercooling in Tunnel 16T (16 ft) than in Tunnel 1T (1 ft), for example. The most recent attempts at developing a kinetic theory model for predicting the amount of supersaturation was done by Pouring (Ref. 2) and applied to one-dimensional flow by Stewart (Ref. 3). The results of the work by Stewart and Pouring show that the theory is computationally complex and would greatly increase the size and computational time of an already complex flow-field code if expanded to two or three dimensions. Therefore, an engineering method of predicting the onset of condensation was developed based on an empirical relationship for the temperature-gradient, supersaturation correlation.

The computer program developed during the investigation reported herein (HUMID/EULER) was used to predict the effects of humidity on several two-dimensional nozzles, two two-dimensional airfoils, a cone at angle of attack, and a three-dimensional (3-D) wing-body combination. The predictions are compared with experimentally determined humidity effects, where the data exist, for validation of the code.

## 2.0 DESCRIPTION OF HUMID/EULER

### 2.1 BASIC EQUATIONS

The computer program developed for calculating the effects of humidity is a modification of an existing Euler solver, designated ARO-1, which is described in detail in Ref. 4.

The five equations solved by the ARO-1 code are the conservation of mass equation, three conservation of momentum equations, and the conservation of energy equation. To calculate the effect of humidity on a flow field, an additional equation was added to represent the conservation of water vapor. The conservation of water vapor equation includes a source term to account for the loss of water vapor caused by condensation. A source term was also included in the energy equation to account for the change in enthalpy attributable to the condensation process. The system of equations for the HUMID/EULER code then becomes

$$\frac{\partial G}{\partial t} + \nabla \cdot F = K \tag{1}$$

where

$$G = \begin{pmatrix} \rho \\ \rho u \\ \rho v \\ \rho w \\ E \\ \sigma \rho \end{pmatrix}$$

$$F = \begin{pmatrix} \rho u & \rho v & \rho w \\ \rho u^2 + P_s & \rho uv & \rho uw \\ \rho uv & \rho v^2 + P_s & \rho vw \\ \rho uw & \rho vw & \rho w^2 + P_s \\ (E + P_s)u & (E + P_s)v & (E + P_s)w \\ \sigma \rho u & \sigma \rho v & \sigma \rho w \end{pmatrix}$$

and

$$K = \begin{pmatrix} 0 \\ 0 \\ 0 \\ -ST_L \\ ST \end{pmatrix}$$

The equation of state is

$$P = (\gamma - 1)\rho e \quad (2)$$

where  $\gamma$  is the ratio of specific heats and  $e$  is the flow internal energy.

HUMID/EULER computations are performed using nondimensional variables constructed to yield stagnation pressure and enthalpy of unity. The stagnation pressure (POI) in atmospheres and stagnation enthalpy (HOI) in Btu/lb are required inputs to the code. The variables introduced in the HUMID subroutine are nondimensionalized in the same manner.

The source term is not necessary on the continuity equation or the momentum equations because the assumption was made that once condensation occurred, the water particles would be transported along with the water vapor. With this assumption, no change in overall mass or momentum would result from condensation. If this assumption were not made, particle-dynamics considerations would be necessary for the water droplets, and a source term for the continuity and momentum equations would then be required.

Like ARO-1, from which this code was developed, HUMID/EULER solves the equations in Cartesian coordinates using a finite-volume approach. The basic numerical algorithm is the explicit, unsplit, predictor-corrector scheme of MacCormack. A detailed description of the basic code, ARO-1, is included in a Users Manual (Ref. 4).

## 2.2 SOURCE TERMS

The source terms on both the conservation of water vapor equation and the energy equation are to represent the change in the flow field introduced by the condensation process. The water vapor source term is

$$ST = \rho(\sigma - \sigma_s) \quad (3)$$

where  $\rho$  is the flow-field density,  $\sigma$  is the local specific humidity, and  $\sigma_s$  is the saturation specific humidity. The term represents the amount of uncondensed water vapor present in the flow field. The energy equation source term is

$$ST_L = \rho(\sigma - \sigma_s)L \quad (4)$$

where  $L$  is the latent heat of vaporization. This term represents the change in total energy as a result of either condensation or revaporization.

## 2.3 CONDENSATION

When water vapor condenses, the latent heat of vaporization is released to the surroundings. Therefore, the effect of local condensation is the addition of energy to the local flow field. A subroutine to compute the energy exchange was established in the code. It was assumed that once the conditions for condensation were met, condensation would occur in such a manner that the specific humidity would be the local saturation value.

The local saturation specific humidity is calculated from the following thermodynamic relationship

$$\sigma_s = 0.6215 [P_{\text{sat}}/(P_s - P_{\text{sat}})] \quad (5)$$

where  $P_s$  is the local static pressure,  $P_{\text{sat}}$  is the saturation vapor pressure, and 0.6215 is the ratio of the molecular weight of water to air. The saturation vapor pressure is calculated using a relationship from Ref. 5.

$$P_{\text{sat}} = 10^{\left(c + \frac{b}{T_s}\right)} (T_s)^a \quad (6)$$

where  $T_s$  is the local static temperature obtained from the internal energy

$$T_s = e/c_v \quad (7)$$

and  $a$ ,  $b$ , and  $c$  are dimensional constants defined in the nomenclature.

A method of predicting the onset of condensation is necessary for the humidity code to be a useful aerodynamic prediction tool. A kinetic theory model of the condensation process is the most accurate method of accounting for the physics of condensation (Ref. 3). However, the theory needs further development to improve its accuracy and computational efficiency; consequentially, an alternate method was sought. An empirical curve fit, Fig. 1, of experimental data reported by Wegener (Ref. 6) was used to establish the conditions at which the onset of condensation occurred. The data provide a relationship between the amount of supercooling,  $T_{\text{ss}}$ , which can exist before condensation effects are observed, and the gradient of static temperature along a streamline,  $dT_s/ds$ . The value of the constant multiplier for  $e$ , -0.075, in the relationship

$$T_{\text{ss}} = [0.408619 (dT/ds) + 50.316944] (1. - e^{-0.075 dT/ds}) \quad (8)$$

is the value required to initiate condensation at the proper  $x$ -location for the Pouring nozzle with a specific humidity of 0.0049. The equation was biased with respect to the data at low

values of  $dT/ds$  to represent the measured minimum  $T_{ss} = 35^\circ\text{F}$  for both the 16T and 16S wind tunnels. Equation (8) is used to predict the onset of condensation for all computations with the code.

The relationship shown for supercooling as a function of  $dT/ds$  in Fig. 1 is truncated at a value of  $T_{ss} = 35^\circ\text{F}$ . The truncation provides a minimum value of  $T_{ss}$ , which is consistent with observed experimental data from the AEDC 16-ft supersonic tunnel nozzle calibration. The minimum value of  $35^\circ\text{F}$  for  $T_{ss}$  will be discussed further in Section 4.1.

The expression  $dT/ds$  is calculated by taking the difference between the local temperature in the computational mesh volume and the local temperature in the neighboring

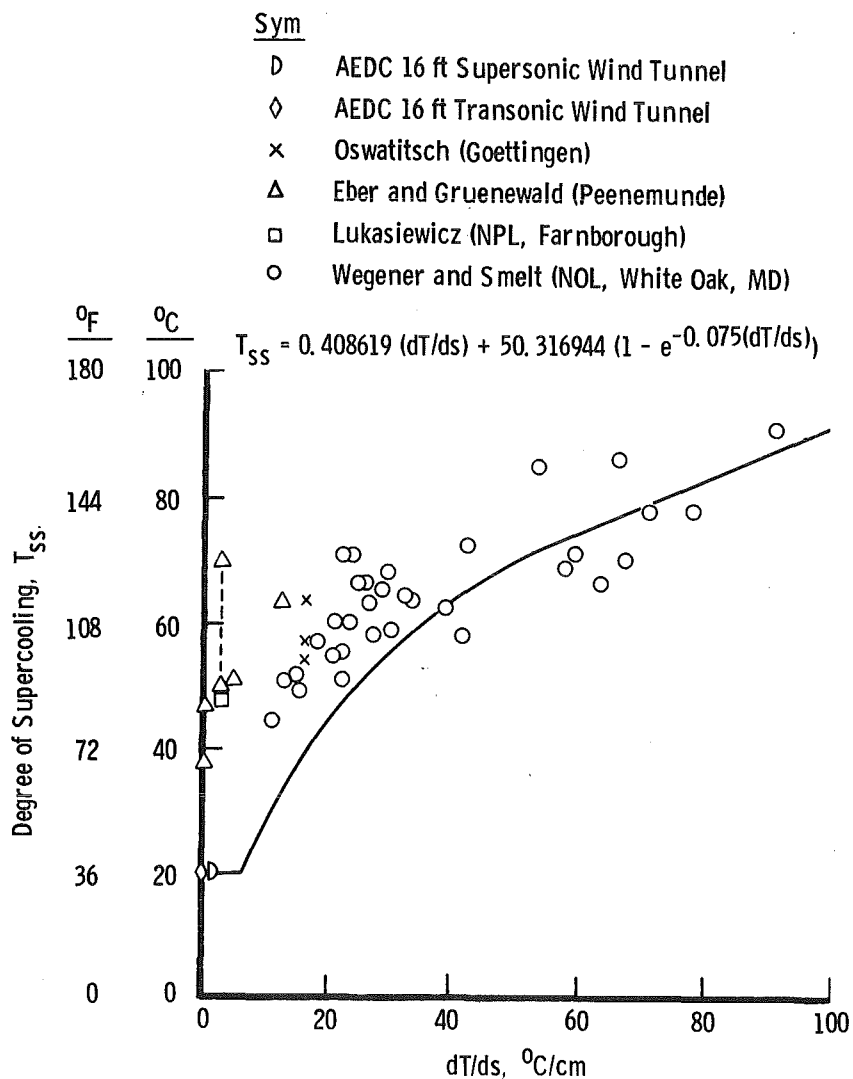


Figure 1. Supercooling as a function of nozzle temperature gradient.

volume in each of the cartesian directions (x, y, and z). The temperature difference is divided by a preselected length scale to calculate  $dT/ds$  for the x, y, and z axes. The three values are then weighted by the local flow angle and summed via the equation.

$$dT/ds = \frac{T_s - T_{sx}}{\Delta x} \frac{u}{U} + \frac{T_s - T_{sy}}{\Delta y} \frac{v}{U} + \frac{T_s - T_{sz}}{\Delta z} \frac{w}{U}$$

The value of  $\Delta x$ ,  $\Delta y$ , and  $\Delta z$  are constant inputs based on model length and the number of mesh points. Thus, for nonuniform meshes, the calculation of  $dT/ds$  with the constant  $\Delta$ 's is not absolutely correct. Modifications are underway to correct that deficiency.

## 2.4 INITIAL AND BOUNDARY CONDITIONS

The parent computer program (ARO-1) provided for initial and boundary conditions to be specified for each geometry or flow-field problem to be solved. This feature has been retained in HUMID/EULER to provide the versatility necessary to address a spectrum of problems. The code requires initial conditions to be specified for each of the flow variables at every mesh point in the computational grid. For the airfoils, the wing body, and the cone, the free-stream Mach number, initial specific humidity, and the conserved variables ( $\rho, \rho u, \rho v, \rho w, E, \sigma q$ ) are specified. The initial condition for the supersonic nozzle assumes the Mach number at the throat is unity. One-dimensional, isentropic-flow assumptions are then used to calculate subsonic and supersonic flow distributions upstream and downstream of the throat, respectively.

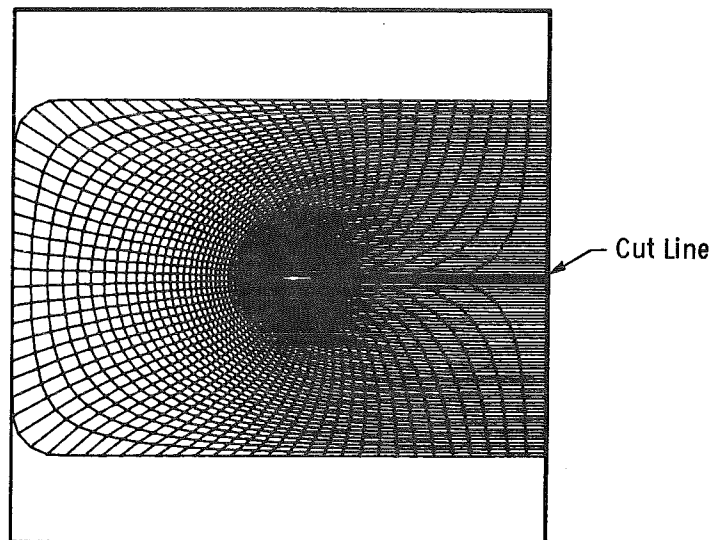
The boundary conditions for the airfoil and the cone are the tangency condition at the model surface. The tangency condition forces a zero gradient across the surface by making the flow-field values in the computational element next to the surface equal to a phantom computational element within the body surface. The boundary conditions on the cut line are equal to field properties in adjacent computational elements across the cut line. The zero-gradient condition is used at the outflow boundary.

The 3-D wing-body combination was computed within a simulated perforated wall wind tunnel. The boundary conditions on the tunnel surface were calculated taking into account boundary-layer growth. For the model surface and symmetry plane, mirror boundary conditions were applied for the mass fluxes with zero normal gradient used for density, energy, and pressure. The downstream boundary condition applies zero gradient for all flow variables except pressure. Pressure was assumed equal to the free-stream value.

Similar boundary conditions are used for the circular arc nozzle with the tangency condition being used on the nozzle surface and the zero-gradient condition at the outflow. The mirror-image condition is applied along the nozzle centerline with characteristic inflow boundary conditions.

### 3.0 COMPUTATIONAL GRID GENERATION

HUMID/EULER requires, as an input, a computational mesh provided from an external source. The grid is dependent on the geometry of the specific problem being computed. All grids used in this study were constructed using grid generators based on solutions of Poisson equations. The grids for the two airfoils (NACA-0012 and the CAST-10) were generated from a code designated GRAPE, which is described in Ref. 7. A C-mesh with 76 x-divisions and 58 y-divisions surrounding the airfoil was chosen. A complete mesh is shown in Fig. 2a, and a close-up view near the airfoil surface is shown in Fig. 2b as a typical example of the airfoil grids.

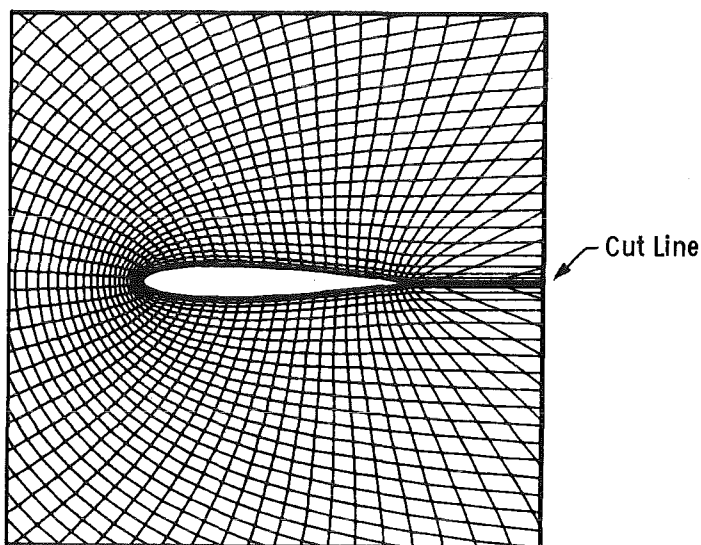


a. Full mesh

Figure 2. Computational mesh for NACA-0012 airfoil.

The mesh for each planar, two-dimensional nozzle was generated using a code designated GRID2D developed by Dr. J. L. Jacocks at AEDC. The nozzle grids contained 100 divisions in the x-direction and 20 divisions in the y-direction. The mesh generated for the Pouring circular arc nozzle is shown as a typical example of the nozzle grids in Fig. 3.

The 3-D grid for the F-16 wing body was developed using the grid generation programs for the wall interference prediction codes (Ref. 8). The codes use input data in the form of



**b. Mesh near airfoil**  
**Figure 2. Concluded.**

axial fuselage and spanwise wing stations and provide a 3-D mesh of a wing-body in a rectangular wind tunnel. The computational grid is generated from the 3-D Poisson equations. The mesh for the grid used in this study has indices of 30 by 31 by 14 in the x, y and z directions. Both the wing-body and the tunnel surfaces have indices of 30 by 31 with 14 grid layers radiating out from the model to the tunnel walls. The wing-body mesh is represented in Fig. 4.

The computational mesh for the sharp-nosed cone in three dimensions was generated by using a simple algebraic code developed by the author. The grid had 38 divisions in the x-direction, ten of which were upstream of the cone nose. There were 13 divisions of the cone surface with 26 layers radiating out from the model. The computational mesh is shown in Fig. 5.

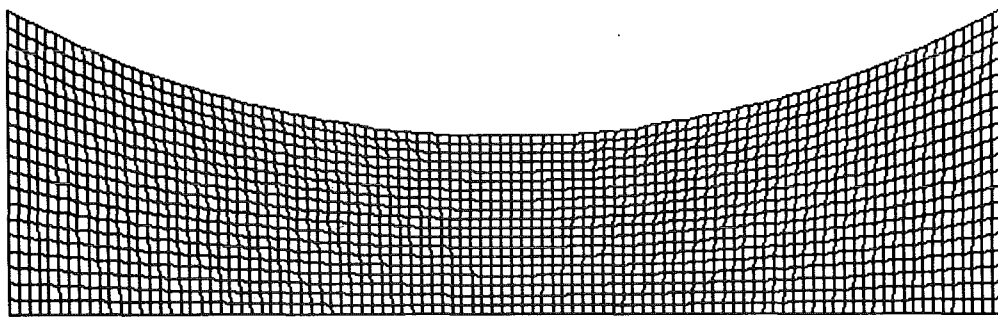


**Figure 3. Computational mesh for circular arc nozzle.**

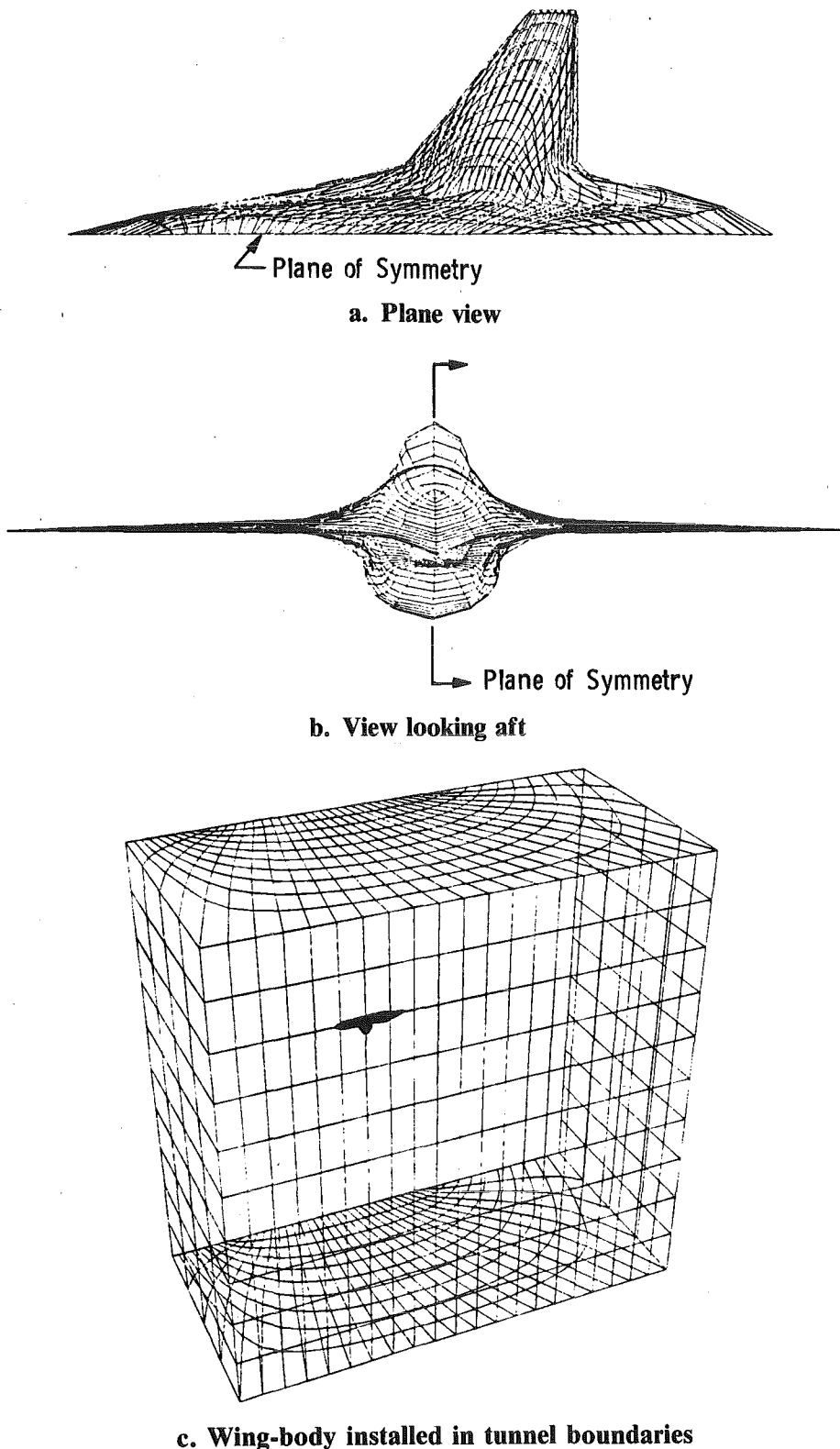
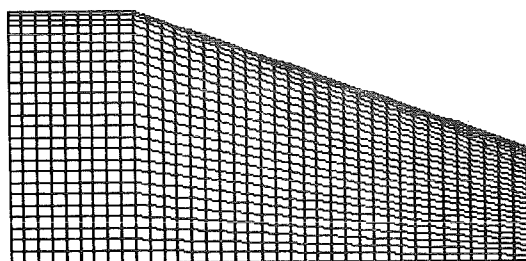
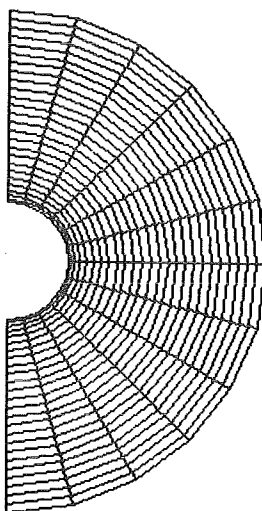


Figure 4. Computational mesh for three-dimensional wing-body.



a. Side view



b. End view at axial position 6 cm

Figure 5. Computational mesh for 15-deg sharp-nosed cone.

## 4.0 DISCUSSION OF RESULTS

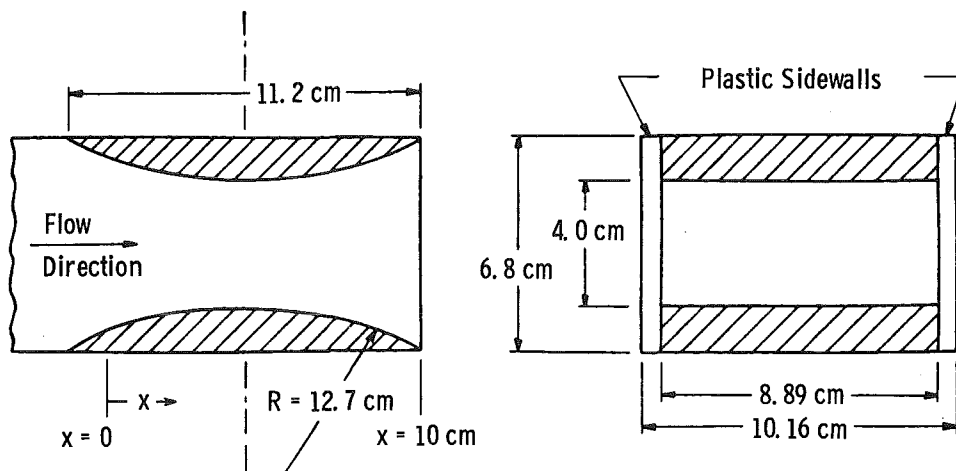
### 4.1 TWO-DIMENSIONAL PREDICTIONS

#### 4.1.1 Nozzles

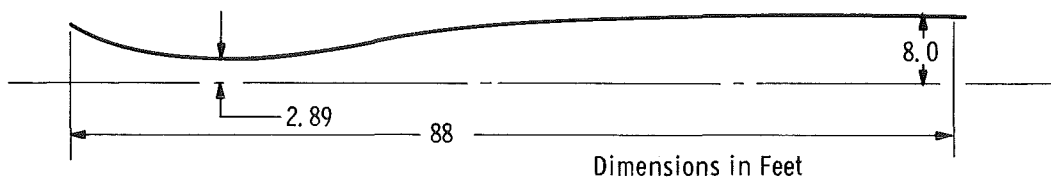
To evaluate the accuracy of the code, it is necessary to compare computational results to experimental data. Since no experimental data could be located for a two-dimensional airfoil, data from other two-dimensional geometries were sought. A series of experimental humidity studies conducted by Pouring (Ref. 2) on a planar, two-dimensional circular arc nozzle and a calibration of the AEDC 16-ft Supersonic Propulsion Wind Tunnel (16S) nozzle provided the desired data. The Pouring nozzle is a planar, two-dimensional, circular arc, Mach 2.1 nozzle with an overall length of 10 cm (Fig. 6a). The small nozzle length provides values of  $dT_s/ds$  on the order of  $100^\circ\text{C}/\text{cm}$ , which result in large values of

supercooling, Fig. 1. The 16S nozzle, on the other hand, is a variable contour nozzle with an overall length of 88 ft (see Fig. 6b for Mach 2.5 contour). This nozzle length results in  $dT_s/ds$  on the order of  $1^\circ\text{C}/\text{cm}$  for a nominal contour of Mach of 2.5 and thereby could not support large values of supercooling.

A comparison of the calculated nozzle centerline pressure distributions with those measured by Pouring for specific humidities of 0.0028, 0.0038, and 0.0049 are presented in Fig. 7. The effect of the energy release in the condensation process is to increase the static pressure and temperature, which results in a decreased Mach number. The prediction obtained from the code agrees well with the experimental results. The two-dimensional flow-field calculations provide the capability of looking at the effect of condensation on the Mach number profile. The Mach number profiles for the Mach 2.1 nozzle are compared for dry flow and a specific humidity of 0.0049 in Fig. 8. The degradation of Mach number caused by the condensation was approximately 5 percent. The condensation line appears in the nozzle flow field on contour plots of the stagnation enthalpy (condensation causes an increase in stagnation enthalpy). The condensation lines shown in Fig. 9 occur at a nozzle Mach number of approximately 1.4.



a. Details and dimensions of the circular arc nozzle geometry



b. 16S nozzle dimensions, Mach 2.5 contour

Figure 6. Two-dimensional nozzles.

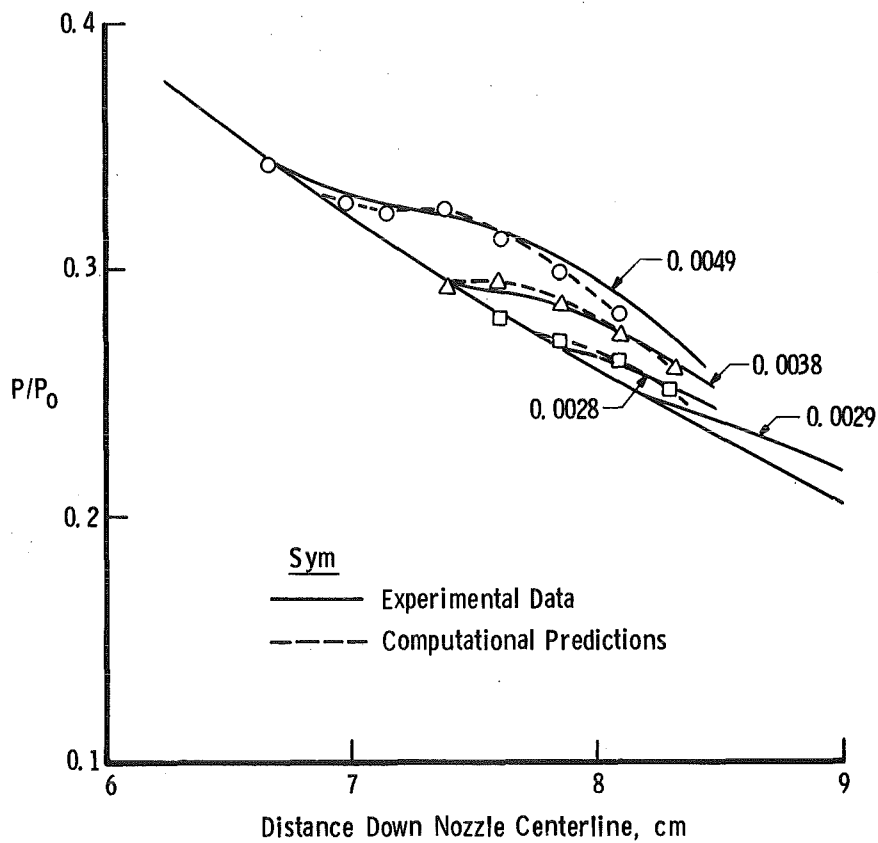


Figure 7. Comparison of predicted condensation effects with experimental results for a Mach 2.1 circular arc nozzle.

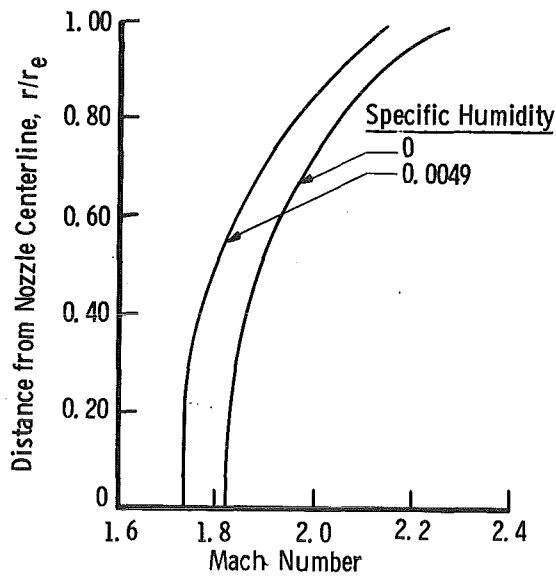
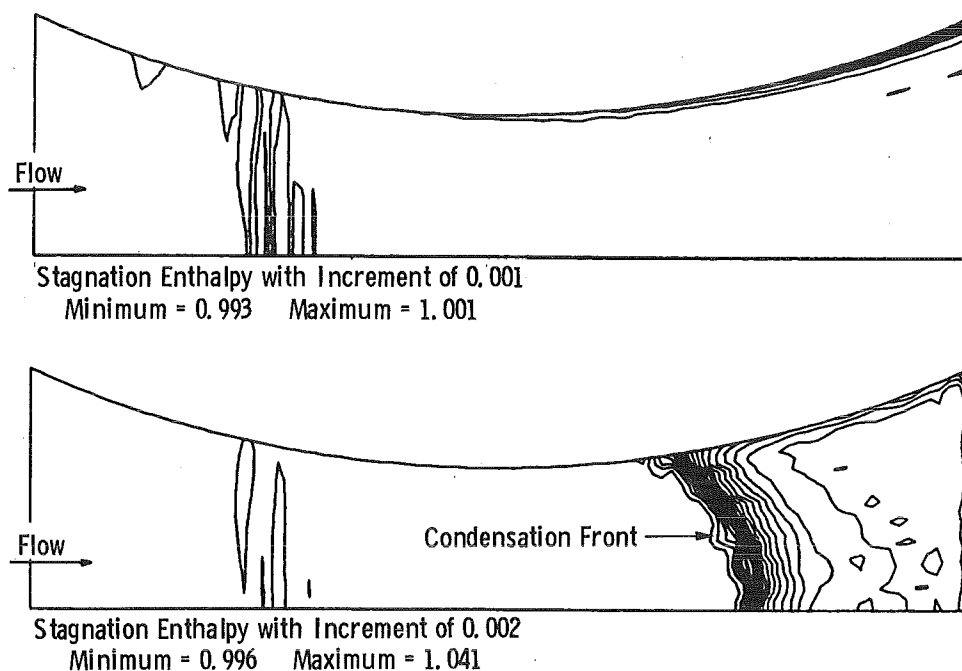


Figure 8. Computed nozzle exit Mach number distribution for specific humidities of 0.0 and 0.0049.



**Figure 9. Computed nozzle total-enthalpy distribution at specific humidities of 0.0 and 0.0049.**

The recent calibration of the AEDC 16-ft Supersonic Propulsion Wind Tunnel (16S) varied specific humidity from 0.0005 to 0.002 at discrete Mach numbers from 1.60 to 3.25. The centerline total pressure along the last quarter of the nozzle was surveyed with a traversing rake. The experimental results from the 16S calibration were corrected and are presented as a function of humidity in Fig. 10 for selected Mach numbers. The predictions of the effect of condensation on the centerline total pressure obtained from HUMID/EULER are also shown. The results from the code show good agreement with the data. The agreement at Mach 2.0 was exact; however, as Mach number increased, the slope of the effect of humidity on nozzle total pressure predicted by the code was larger than measured. It should be pointed out that no consideration of the nozzle boundary layer was provided in the code. A representative nozzle total-enthalpy profile is shown in Fig. 11.

The experimental results from the Mach 1.6 nozzle contour showed no effect of humidity on the centerline pressures at specific humidities below 0.001 (Fig. 10). This lack of effect implied that a minimum supercooling value exists below which no condensation effects will be observed. This minimum was determined to be 35°F and was input into the code through the relationship between  $dT_s/ds$  and supercooling (Fig. 1). This minimum value gave the desired effect at Mach 1.6 and has been retained in all calculations made with the code.

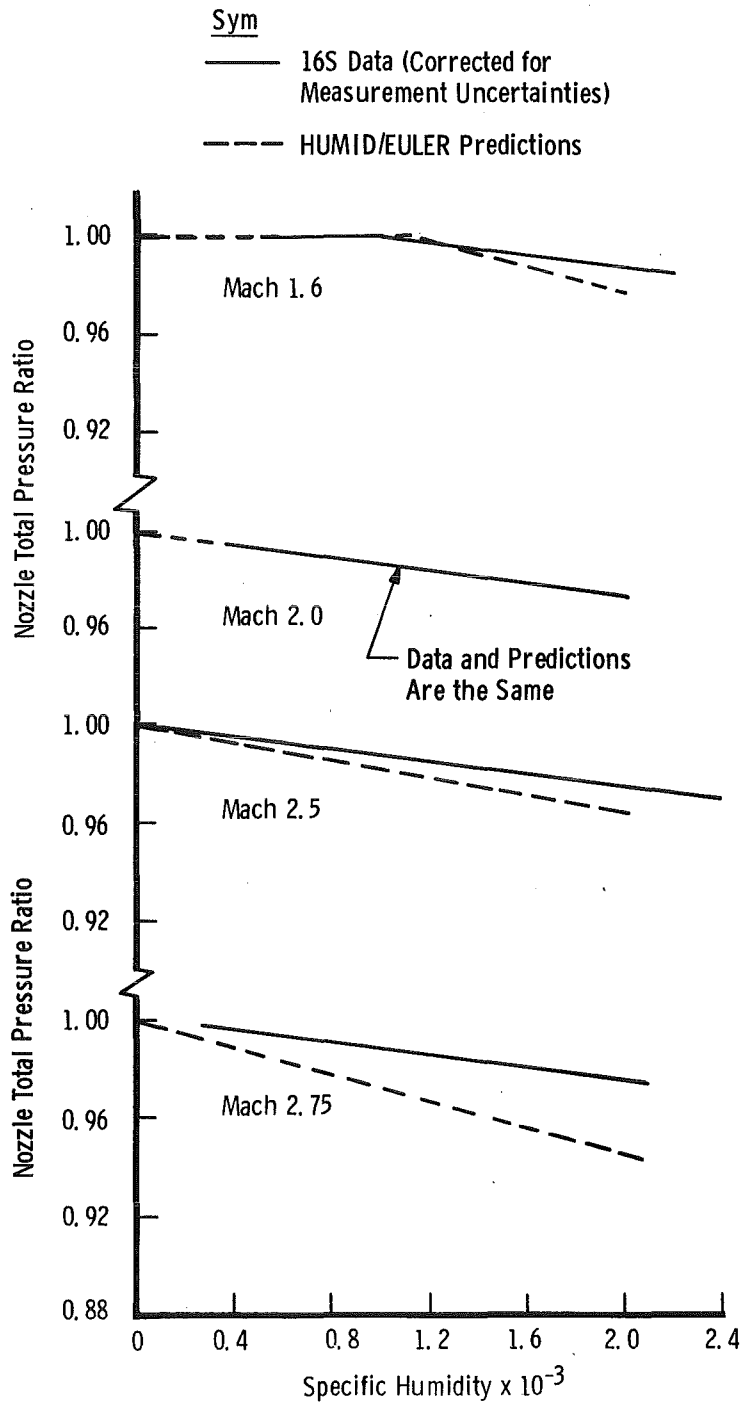


**Figure 10. Effect of humidity on 16S nozzle total pressure.**

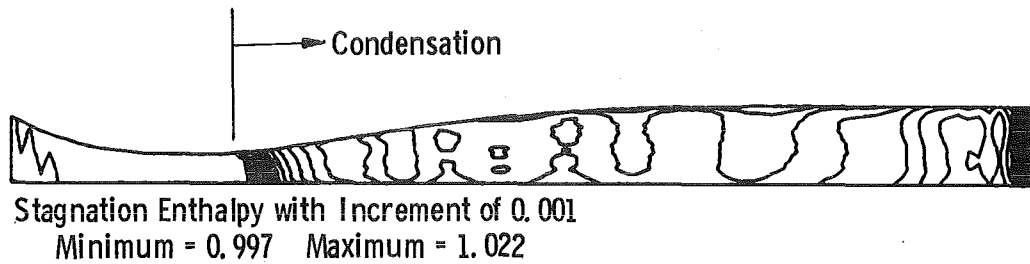
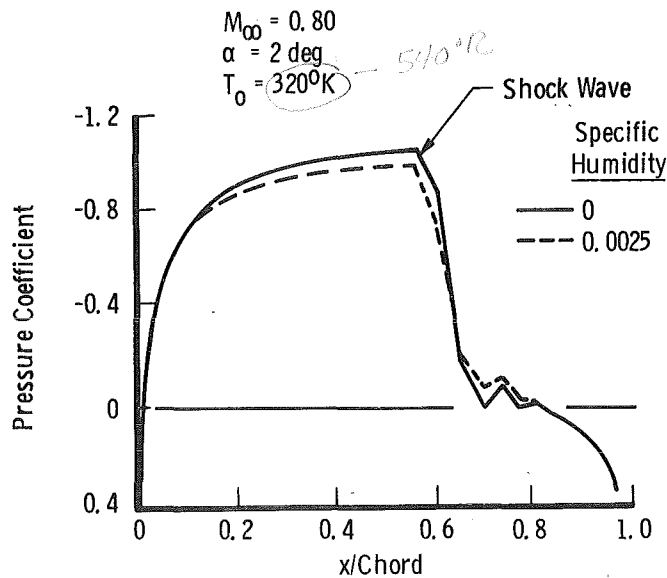


**Figure 11. Computed nozzle total-enthalpy distribution at a specific humidity of 0.002 for the 16S Mach 2.5 contour.**

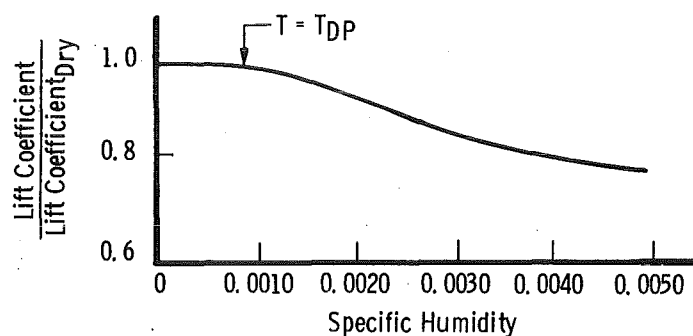
**4.1.2 Airfoils**

HUMID/EULER is being developed to predict the effects of local condensation on the aerodynamic parameters of wind tunnel models. The two-dimensional code was used to assess the effect of local condensation on two airfoils at transonic conditions, the NACA-0012 and the CAST-10. There are no experimental data with controlled specific humidity available for the airfoils; therefore, humidity effects are discussed in relation to the “dry” solution for each flow condition.

The steady-state flow field about an NACA-0012 airfoil with free-stream Mach number of 0.8 and an angle of attack of 2 deg was calculated for specific humidities ranging from 0 to 0.005. The pressure distributions on the upper surface of the airfoil at  $\sigma = 0$  and 0.0025 are compared in Fig. 12a. The effect of local condensation is to increase the pressure on the



**a. Upper surface pressure profile**  
**Figure 12. Humidity effects on an NACA-0012 airfoil.**



**b. Normal-force coefficient**  
**Figure 12. Concluded.**

airfoil upstream of the shock wave. The shock location also moves slightly upstream with condensation (Fig. 13) and the pressure recovery across the shock is less. The calculated pressure distribution on the airfoil was integrated to determine the aerodynamic coefficients. The effect of varying humidity on the normal-force coefficient is shown in Fig. 12b. The coefficient decreases 23 percent from the value calculated for a dry flow field as humidity increases to 0.0050. The relationship has an inflection point near a specific humidity of 0.0025, at which the rate of the change of  $C_L$  with  $\sigma$  decreases. Further analysis of the computational data suggests a possible explanation for the inflection point. The condensation pressure and temperature increases with increasing humidity, according to the relationship in Equations (5) and (6). As specific humidity increases from zero, with all other independent variables held constant, condensation will occur first at the minimum pressure on the airfoil and will move forward to regions of higher pressure as humidity increases. The variation of the point at which condensation started for the range of specific humidities calculated is shown in Fig. 14a. The shock location also moves forward with increasing humidity; however, the mesh size used in the calculations precludes the resolution of shock position. However, as an indication of shock position, the percent change in Mach number from the calculated value at the mesh point upstream of the shock to the calculated value at the next mesh point was used to quantify the shock movement (Fig. 14b). As specific humidity increases from 0, the percent change in Mach number across the mesh spacing increases from 10 percent at  $\sigma = 0.0$  to 13 percent at  $\sigma = 0.0025$ . Above a specific humidity of 0.0025, the Mach number change across the mesh spacing is constant at 13 percent, indicating a stationary shock position. Thus, at low values of humidity,  $C_L$  as a function of  $\sigma$  is influenced by the combination of decreasing pressure and forward shock movement. At  $\sigma$  about 0.0025, the shock location then becomes constant, and the rate of change of  $C_L$  is reduced for higher values of specific humidity, thereby causing the inflection at  $\sigma$  near 0.0025 shown in Fig. 12b.

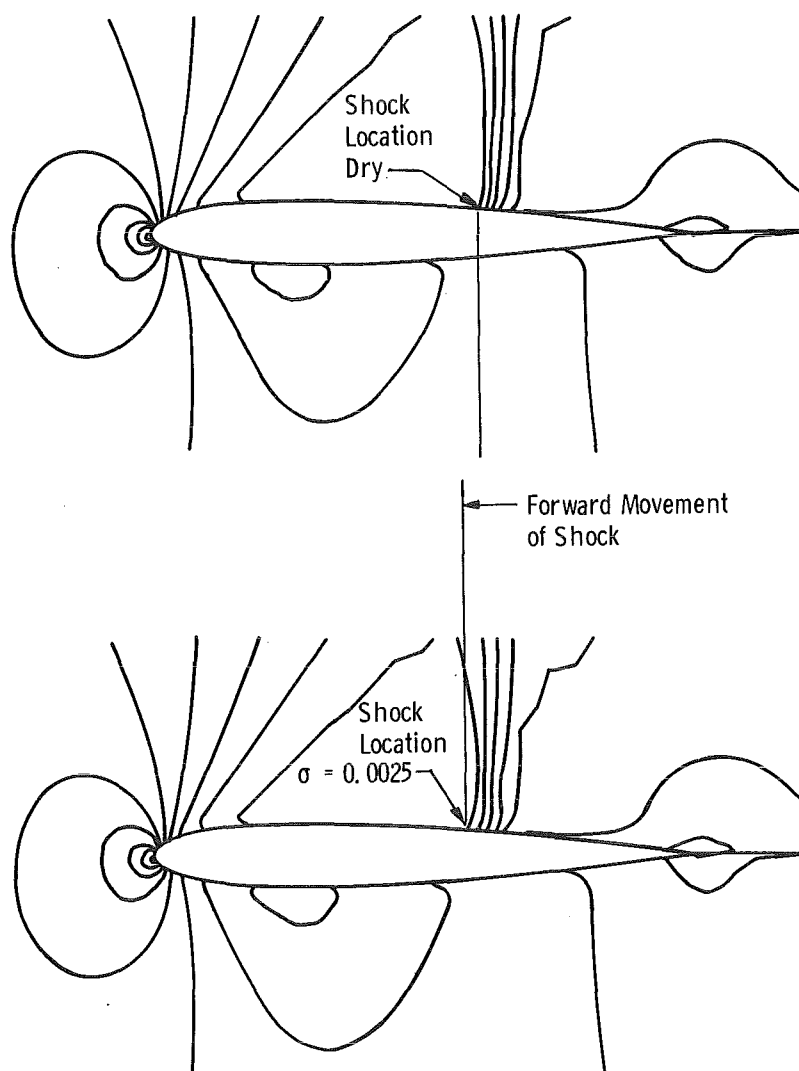
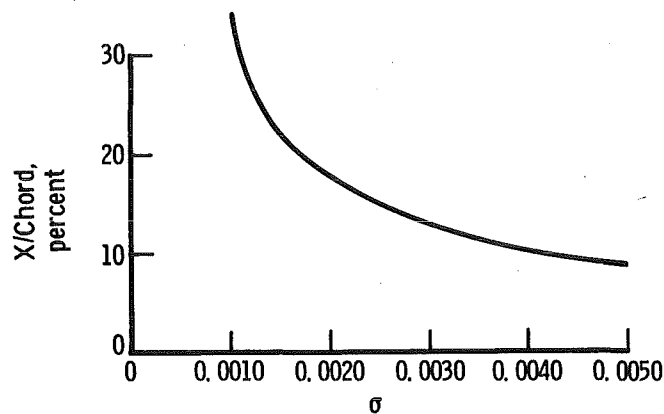


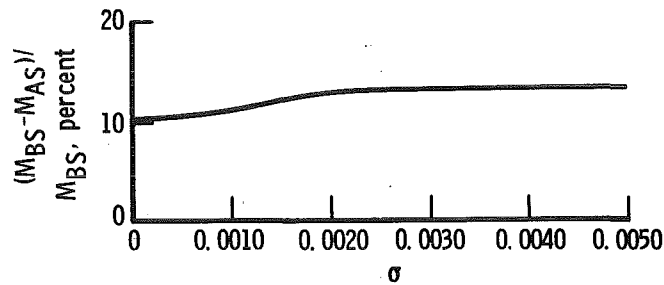
**Figure 13. Effect of local condensation on Mach number contours.**

As in the nozzle calculations, condensation patterns can be visualized on contour plots of total enthalpy. The enthalpy contours for the NACA-0012 airfoil at a specific humidity of 0.0025 is shown in Fig. 15.

Calculations of the effects of condensation at a specific humidity of 0.0040 were made on a transonic airfoil (CAST-10) geometry (Fig. 16). Several calculations were made at Mach 0.765,  $\alpha = 2.85$ , with the only variable being the length of the chord. This calculation provides the effect of scale on the humidity effect. The normal-force coefficient, normalized



a. Location of condensation onset



b. Ratio of Mach number across mesh volume containing shock

Figure 14. Condensation onset location and percent Mach number decrease after shock as a function of specific humidity.

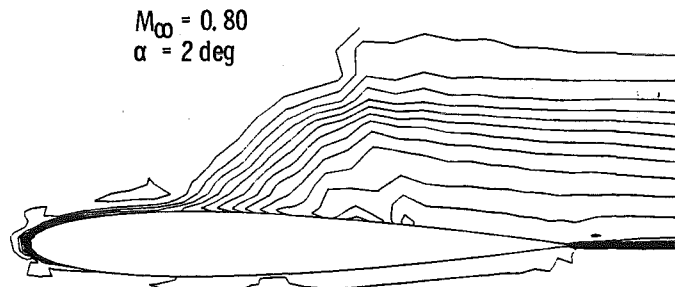


Figure 15. Computed nozzle total-enthalpy distribution at a specific humidity of 0.0025 for the NACA-0012 airfoil.

to the dry value, is presented as a function of chord length in Fig. 17. For this range of model sizes, the maximum effect of condensation (approximately 7 percent reduction in  $C_l$ ) is reached at a chord length of 8 cm. At model sizes above 8 cm, the effect of condensation is essentially constant. The variation of condensation effects with chord length demonstrates that more attention must be given to the wind tunnel moisture content to obtain influence-free data for the larger scale models. However, when the model geometric parameters, such

as chord length, are on the order of the rate kinetics of condensation scale, the maximum effect is attained and remains essentially constant as the scale is increased.

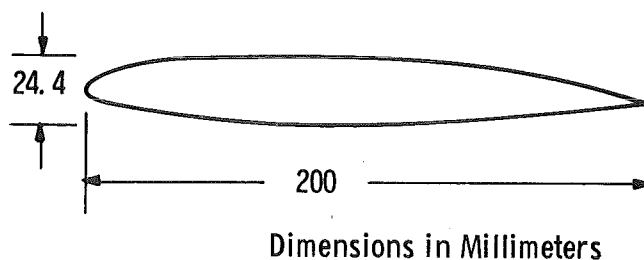


Figure 16. Profile of Cast-10 transonic airfoil.

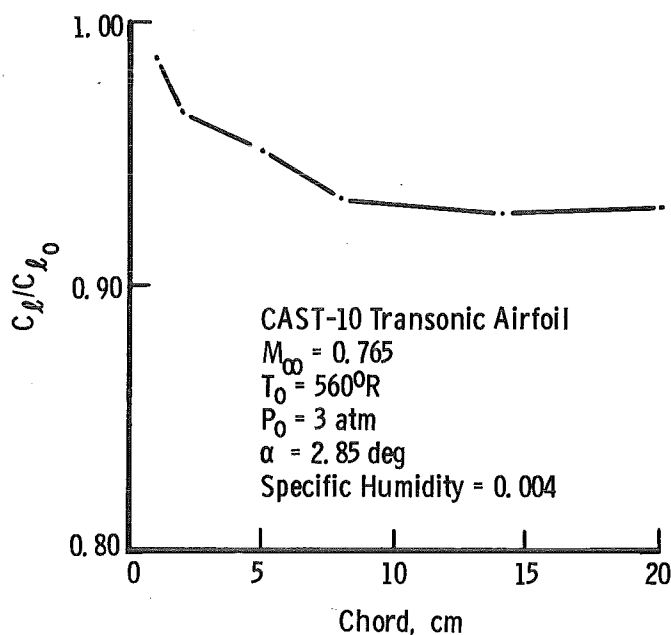


Figure 17. Effect of model scale on normal-force coefficient at constant specific humidity.

#### 4.1.3 Aerodynamic and Propulsion Test Unit (APTU) Predictions

The APTU, located at AEDC, is a blowdown type of freejet test facility consisting of a supersonic nozzle exhausting into a cylindrical duct that exits through a downstream jet pump to atmosphere. The APTU facility is designed to match temperature and pressure conditions over a wide range of altitudes.

The APTU nozzles have flow conditions with high total pressures and temperatures. Typical nozzle flow stagnation conditions for the Mach 3.5 nozzle are 8.8 atm pressure and

1345°R temperature. The mass flow is heated to the high temperatures using a butane heater. The combustion process introduces specific humidities of 0.0125 into the nozzle flow at the stated conditions. These flow conditions for the Mach 3.5 nozzle were chosen for flow-field predictions using HUMID/EULER. The size of the axisymmetric APTU nozzle (Fig. 18) is between the Pouring nozzle and the Tunnel 16S nozzle.

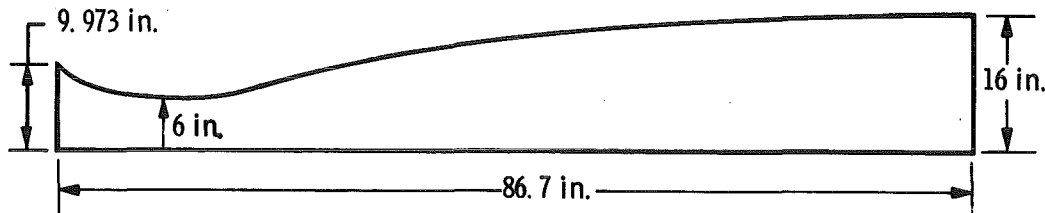
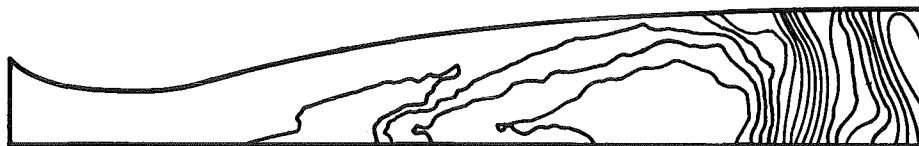


Figure 18. Geometry of APTU Mach 3.5 nozzle.

The condensation line in the APTU nozzle is not as sharp as observed in the previous nozzle (Fig. 19). This difference is caused by the variation of the latent heat of vaporization with temperature by an empirical fit of the steam table,

$$L = 41.443 (1165.47 - T_s)^{1/2} e^{8.3243 \times 10^{-7} (T_s - 492)^2} \quad (10)$$



Stagnation Enthalpy with Increment of 0.008  
 Minimum - 0.868      Maximum - 1.027

Figure 19. Computed nozzle total-enthalpy distribution at a specific humidity of 0.012 for the APTU Mach 3.5 contour.

At static temperatures in excess of 707°R, the latent heat of vaporization is 0. The reduced value of the latent heat decreases the impact that condensation has on the nozzle flow properties. The effect is quantified in a comparison of the nozzle exit Mach number profiles for the humid and the dry-flow predictions (Fig. 20). The maximum effect is near the centerline of the flow where the condensation is concentrated. At a temperature of 1800°R the code predicts that condensation will not occur.

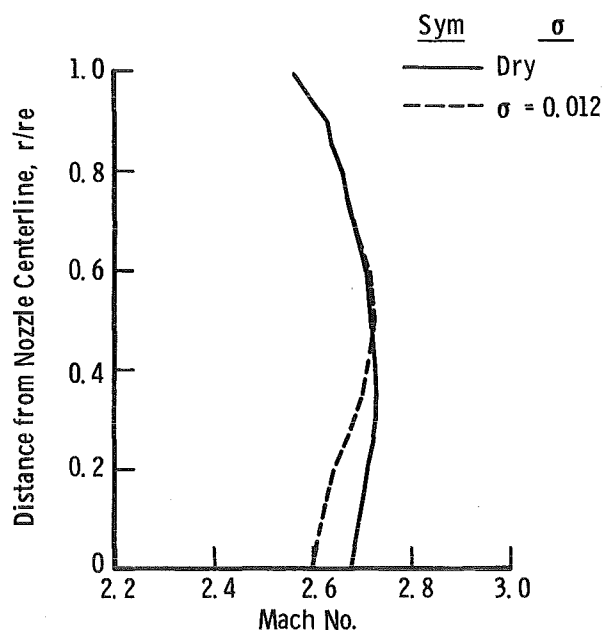


Figure 20. Computed nozzle exit Mach number distribution for specific humidities of 0.0 and 0.0120, Mach 3.5 APTU nozzle.

## 4.2 THREE-DIMENSIONAL PREDICTIONS

Wind tunnel models usually tested in the AEDC tunnels are 3-D. Therefore, HUMID/EULER must be capable of providing humidity effect predictions in three dimensions to attain the desired utility. The predictions of the flow field about a sharp-nosed cone at angle of attack and a wing-body combination representative of the F-16 were chosen to demonstrate the capability of the code in three dimensions.

### 4.2.1 Cone Predictions

Cones are used extensively in the calibration of the AEDC wind tunnels. In the supersonic tunnels such as Tunnels A and B, a different aspect of the humidity problem must be considered. Assuming that the moisture in the flow field condensed in the nozzle, the question arises as to what will be the effect on the model measurements if the moisture revaporizes. Revaporization removes from the flow field the latent heat of vaporization, thereby reducing the temperature. Across a shock the pressure will increase, which will

provide an increased saturation specific humidity [Eqs. (5) and (6)]. The code allows moisture to revaporize to the saturation value provided the saturation value does not exceed the initial specific humidity of the flow field. The initial specific humidity is equivalent to the entire moisture in the flow field.

Predictions of the effects of revaporization were made with HUMID/EULER for cones of 15- and 7.5-deg half angles at Mach numbers of 1.15 and 2.18, respectively. To show the 3-D capability of the code, the calculations were made a 2-deg angle of attack. The predictions of the cone surface parameters with revaporization are compared to the "dry" calculations.

The Mach number behind the shock for the 15-deg cone at  $M_\infty$  of 1.15 is subsonic. The saturation specific humidity increased from 0.0006 to 0.00135, which caused an increase in the Mach number on the cone surface compared to the dry condition as shown in Fig. 21. The 0-deg element represents the lee side of the cone at 2-deg angle of attack, the 90-deg element is the side of the cone, and the 180-deg element is the windward side. The variation of Mach number and pressure coefficient is presented in Fig. 22 for the lee side of the cone.

The 7.5-deg cone at a free-stream Mach number of 2.18 has supersonic flow downstream of the shock. As shown in Fig. 23, no large effects of revaporization were predicted. The saturation specific humidity increased from  $9.2 \times 10^{-9}$  to  $4.4 \times 10^{-8}$  (a ratio of approximately 5) on the lee side. However, the total amount of energy available at this low value of specific humidity is insignificant and has only a small influence on the predicted surface Mach numbers. The effect of revaporization on the surface Mach number for the 7.5-deg cone is opposite in sign from the effect predicted on the 15-deg cone. The reversal of the humidity effect is expected since the physical process is one of heat addition to a flow field. The effect of heat addition is to drive the flow toward Mach 1 from either a subsonic or a supersonic initial condition.

The previous calculations show the HUMID/EULER can reasonably address the effects of revaporization on cones. Depending on the flow-field parameters and the cone geometry, the effect of revaporization can either be large or very small.

#### 4.2.2 Wing-Body Predictions

The three-dimensional wing-body chosen to demonstrate the HUMID/EULER capability was a representation of the F-16. This model was chosen because of the availability of some experimental data for code validation. The calculations were made at a free-stream Mach number of 0.9 and angles of attack of 0- and 6-deg. The predictions are presented in Fig. 24 as the change in lift coefficient at a humidity value of 0.0005 to a higher

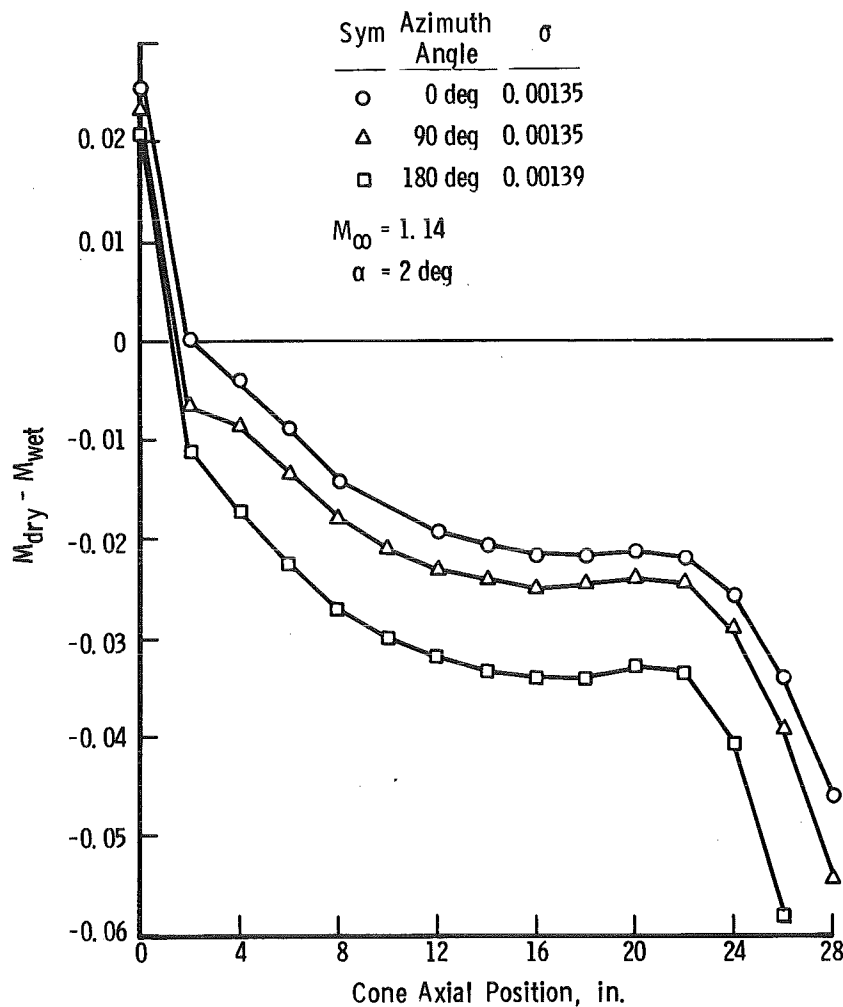
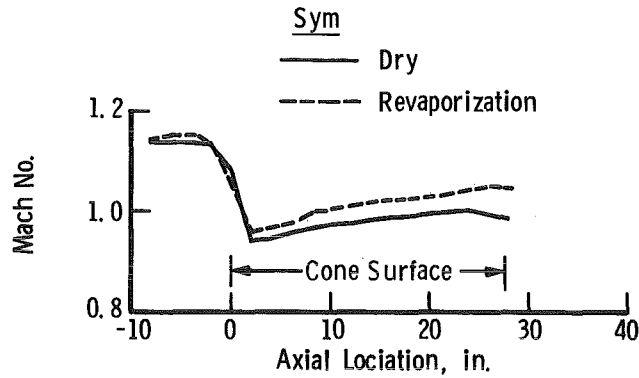


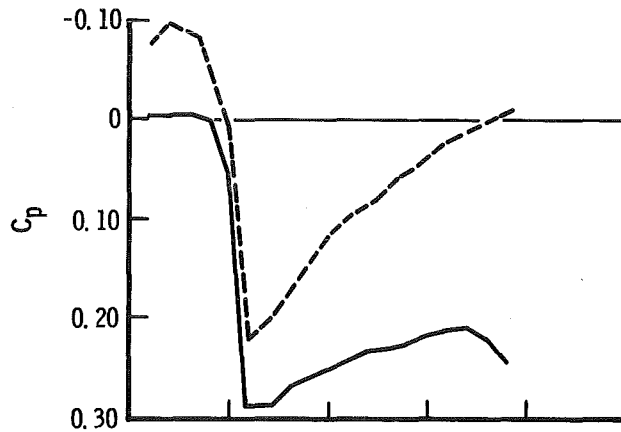
**Figure 21. Comparison of Mach number of 15-deg cone surface with and without revaporization.**

value versus the parameter ( $T_\infty - TDP$ ). The experimental data from the F-16 at an angle of attack of 6-deg, Ref 9, are also included. The predicted effect of humidity on lift coefficient agrees reasonably well with the experimental data, Fig. 24a. The reversal of the predicted effect at values of ( $T_\infty - TDP$ ) less than  $-5^\circ R$  is not understood. As expected the effect of condensation on lift at 6-deg angle of attack is more pronounced than at 0-deg, Fig. 24b. The predicted effect on the axial force coefficient ( $C_A$ ) is in the opposite direction and of much greater magnitude than reported in the data (Fig. 24c), however, the onset of the predicted effect agrees with the experimental observations. The disagreement of the computational results and the experiment can possibly be attributed to the coarseness of the computational mesh. For example, the wing is represented by only 18 chordwise mesh lines whereas 100 to 150 would be required for good drag resolution.

The humidity effect is caused by local condensation in the near flow field of the model. Therefore, to more accurately predict the effect, a fine mesh on the model surface is desirable. While mesh used for the F-16 calculations is very coarse, it represents the state of the art in 3-D single mesh generation. Further improvements in the development of computational meshes should improve the accuracy of humidity effect predictions on wing-body configurations.



a. Mach number



b. Pressure coefficient

**Figure 22. Mach number and pressure coefficient distribution on lee side of 15-deg cone at a free-stream Mach number of 1.15 with and without revaporization.**

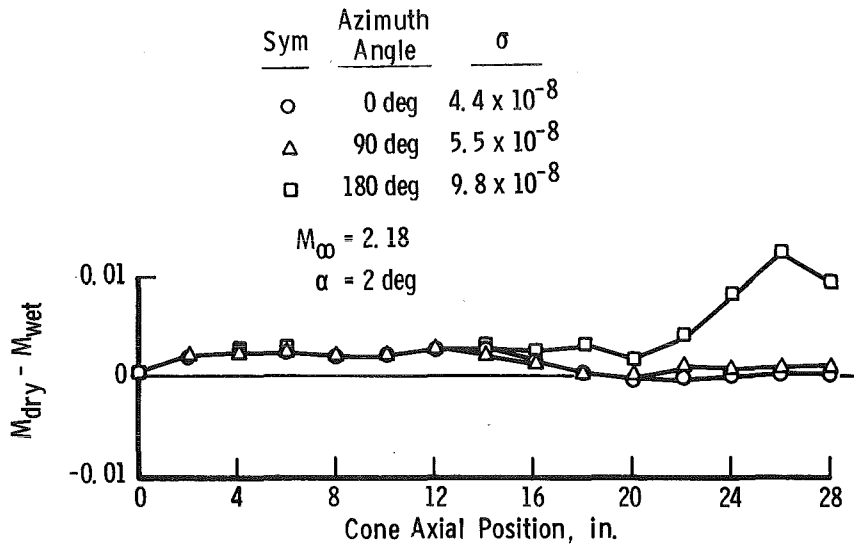


Figure 23. Comparison of Mach number on 7.5-deg cone surface with and without revaporization.

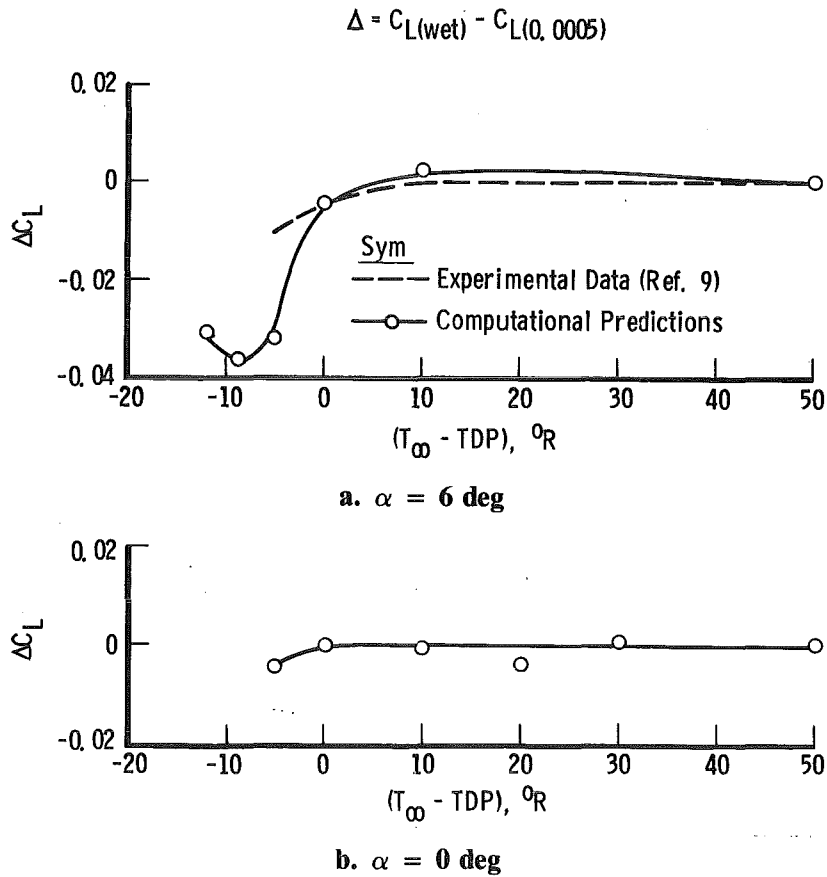
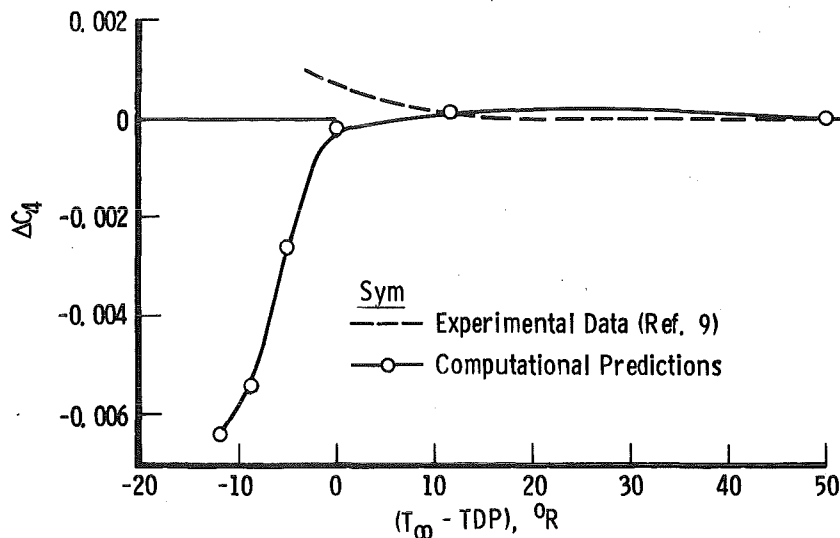


Figure 24. Humidity effects on an F-16 wing-body as a function of dew point temperature.



c. Axial force coefficient,  $\alpha = 6$  deg  
 Figure 24. Concluded.

## 5.0 CONCLUSIONS

HUMID/EULER has been developed to predict the effect of moisture condensation on aerodynamic flow fields. An empirical relationship between supercooling and the rate of change of flow-field temperature was developed to provide a criteria for the onset of condensation. The code has been applied to several nozzle configurations, two two-dimensional airfoils, and a cone at angle of attack. The conclusions drawn from the code results are:

1. The computed effect of condensation on the pressure along the two-dimensional nozzle centerlines agree with the experimental data available from the Pouring and the AEDC 16-ft Supersonic Propulsion Wind Tunnel nozzles. The good agreement with experiment for such vastly different size nozzles demonstrates the range of applicability of the code.
2. The effect of condensation on the flow field of the Mach 3.5 APTU nozzle was less than the effect on the 16S nozzles. The reduced effect was a result of the small value for the latent heat of vaporization at the high temperature and pressure conditions of the APTU nozzle.

3. With a free-stream specific humidity of 0.005, Mach number 0.8, and 2-deg incidence, condensation on the NACA-0012 airfoil reduces the lift coefficient 23 percent from the value calculated for dry flow. The shock location moves slightly forward at the Mach 0.8, alpha equal 2-deg condition.
4. The effect of model scale on condensation influences was demonstrated on the CAST-10 transonic airfoil. The lift coefficient decreased with increasing chord length to a value of 93 percent of the dry value at a chord length of 8 cm. At chord increases beyond 8 cm, no changes in condensation effect were predicted.
5. The effect of revaporization on the surface Mach number of a cone at angle of attack is more pronounced on the windward surface. For the conditions investigated, the largest effect of revaporization occurs on a cone that has subsonic flow downstream of the nose shock.
6. The humidity effects predicted with HUMID/EULER for the F-16 configuration agree reasonably well with the experimental measurements of humidity effects at Mach 0.9. The agreement probably can be improved with increased fineness of the computational mesh on the model surface.

#### REFERENCES

1. Lukasiewicz, Julius and Royle, J. K. "Effect of Air Humidity in Supersonic Wind Tunnels." A.R.C. Technical Report No. 2563, 1953.
2. Pouring, A. A. "An Experimental and Analytic Investigation of Homogeneous Condensation of Water Vapor in Air During Rapid Expansions." Ph.D Dissertation, Yale University, 1963.
3. Stewart, V. W. III. "A Kinetic Theory Approach to Computation of Supersonic Nozzle Flow with Water Vapor Condensation." Masters Thesis, University of Tennessee, August 1983.
4. Koenig, K. and Barton, J. M. "Numerical Solution of the Three-Dimensional Unsteady Euler Equations." AEDC-TR-83-22 (AD-A132 034), August 1983.

5. Parish, O. O. and Putnam, T. W. "Equations for the Determination of Humidity from Dewpoint and Psychrometric Data." NASA-TND-8401, January 1977.
6. Wegener, Peter P., ed. *Nonequilibrium Flows, Part I*. Marcell Dekker, Inc., New York, 1969.
7. Sorenson, R. L. "A Computer Program to Generate Two-Dimensional Grids About Airfoils and Other Shapes by the Use of Poisson's Equation." NASA Technical Memorandum 81198.
8. Suhs, N. E. "Computational Estimations of Strut Support Interference at Transonic Mach Numbers." AIAA-85-5018, AIAA 3rd Applied Aerodynamics Conference, October 15-16, 1985.
9. Lucas, Ernest J. "Model Size and Humidity Effects on Selected Calibration Parameters for the 16-ft Transonic Wind Tunnel at AEDC." AEDC-TR-81-17 (AD-A107728), November, 1981.

## NOMENCLATURE

a	-4.92830	} Dimensional constants for Eq. (5)
b	-5287.32	
c	23.2801	
$C_l$	Airfoil lift coefficient	
$C_p$	Pressure coefficient $(C_p - p_\infty)/q_\infty$	
$C_v$	Specific heat of air at constant volume, 0.1716 Btu/lb	
E	Total energy, $\rho(e + q^2/2)$	
e	Local internal energy, $C_v T$ , Btu/lb	
F	Tensor of fluxes, Eq. (1)	
G	Vector of dependent variables, Eq. (1)	
K	Source term of Eq. (1)	
L	Latent heat of vaporization, 1055 Btu/lb	
$M_{dry}$	Mach number on cone surface behind shock, no humidity	
$M_{wet}$	Mach number on cone surface behind shock, with revaporization	
$M_\infty$	Free-stream Mach number	
$P_o$	Stagnation pressure, atm	
$p_s$	Local static pressure, atm	
$p_{sat}$	Local saturation pressure, atm	
q	$(u^2 + v^2 + w^2)$	

$r$	Radius of circular arc nozzle
$r_e$	Radius of circular arc nozzle at exit
$ST$	Water vapor source term, Eq. (3)
$ST_L$	Energy source term, Eq. (4)
$s$	Distance along streamline, cm
$TDP$	Dewpoint temperature
$T_o$	Local stagnation temperature, °R
$T_s$	Local static temperature, °R
$T_{ss}$	Degree of supercooling, $(TDP - T_s)$ , °C, Fig. 1
$T_\infty$	Free-stream static temperature, °R
$u$	Velocity component, x-direction
$v$	Velocity component, y-direction
$w$	Velocity component, z-direction
$x_N$	Distance along nozzle centerline
$x$	} Axis designation, cartesian coordinates
$y$	
$z$	
$\alpha$	Angle of attack, deg
$\rho$	Local density in flow field
$\sigma$	Specific humidity, lb H <sub>2</sub> O/lb air
$\sigma_s$	Saturation specific humidity